A New Adaptive Interpolation Algorithm for 3D Ultrasound Imaging with Speckle Reduction and Edge Preservation

Qinghua Huang[a,c], Minhua Lu[d], Yongping Zheng[b,c], Tianfu Wang[d], and Siping Chen[d]

[a] School of Electronic and Information Engineering, South China University of Technology, Guangzhou, Guangdong, P.R.China.

[b] Research Institute of Innovative Products & Technology, The Hong Kong Polytechnic University, Hung Hom, Kowloon, Hong Kong SAR, P.R.China.

[c] Department of Health Technology and Informatics, The Hong Kong Polytechnic University, Hung Hom, Kowloon, Hong Kong SAR, P.R.China.

[d] Department of Biomedical Engineering, Shenzhen University, Shenzhen, Guangdong, P.R.China.

Running Title: Adaptive interpolation in 3D ultrasound

Corresponding author: Qinghua Huang, PhD. Email: **qhhuang@ieee.org**

Abstract

Conventional interpolation algorithms for reconstructing freehand three-dimensional (3D) ultrasound data always contain speckle noises and artifacts. This paper described a new algorithm for reconstructing regular voxel arrays with reduced speckles and preserved edges. To study speckle statistics properties including mean and variance in sequential B-mode images in 3D space, experiments were conducted on an ultrasound resolution phantom and real human tissues. In the volume reconstruction, the homogeneity of the neighborhood for each voxel was evaluated according to the local variance/mean of neighboring pixels. If a voxel was locating in a homogeneous region, its neighboring pixels were averaged as the interpolation output. Otherwise, the size of the voxel neighborhood was contracted and the ratio was re-calculated. If its neighborhood was deemed as an inhomogeneous region, the voxel value was calculated using an adaptive Gaussian distance weighted method with respect to the local statistics. A novel method was proposed to reconstruct volume data set with economical usage of memory. Preliminary results obtained from the phantom and a subject's forearm demonstrated that the proposed algorithm was able to well suppress speckles and preserve edges in 3D images. We expect that this study can provide a useful imaging tool for clinical applications using 3D ultrasound.

Keywords: 3D ultrasound imaging; Interpolation; Volume reconstruction; Adaptive Gaussian distance weighted; Speckle reduction; Edge preservation

1. Introduction

Ultrasound has been recognized as the most often used imaging tool in clinical environments. Conventional 2D ultrasound imaging has limitations in 3D structural analysis, especially for volume quantification and tissue localization, which are necessary in assessing the progression of disease and uncovering the properties of human tissues. Thus, attention has been paid to developing 3D ultrasound imaging which has been recognized as a promising evaluation tool for a variety of clinical applications since the 1980s [1-3].

In past decades, lots of researchers have proposed techniques for reconstruction and visualization of 3D ultrasound images from echo data. To date, they can be mainly grouped into two main categories: real-time imaging using a 3D probe and 3D imaging based on a set of conventional 2D ultrasound images (B-scans). Dedicated 3D probes usually consist of 2D arrays that allow explicit 3D imaging [4]. Several commercial types of 3D probes make use of an internal mechanical motor to drive an annular array for accurate scanning within the probe housing. However, these 3D probes are relatively large and expensive. Their image resolution was not as good as conventional ultrasound image. Furthermore, the field of view of such dedicated 3-D probes was limited by the dimensions of piezoelectric elements in the probe.

In contrast, the 3D imaging methods based on conventional B-scans provide inexpensive solutions for medical diagnoses by locating individual B-scans in space using mechanical scanning apparatus or spatial sensing devices. Dating back to the 1980s and early 1990s, many seminal 3D ultrasound systems adopted a mechanical probe mover to control the motion of a conventional ultrasound probe and to record the positions and orientations of B-scans [5-9] during the moving process of the probe. This method can be viewed as one of the most original ideas in producing 3D ultrasound images and now is adopted for designing various types of 3D real-time volumetric probes [10, 11]. Although the mechanical scanning worked well in obtaining high-quality 3D images and conducting fast reconstructions, earlier scanning apparatus were bulky and inconvenient to use for different applications [1]. Since the early 1990s, freehand scanning methods which provide much more flexibility have been widely used to overcome the shortcomings of their mechanical scanning counterparts. Freehand 3D imaging systems allow image acquisition with unconstrained movement [1, 2, 12]. Generally, they make use of a spatial tracking sensor attached to an ultrasound probe for capturing spatial information of the B-scans in real-time. The tracking sensors that have been used for numerous tracked freehand systems in the past decades include electromagnetic sensing devices [13], acoustic spark gaps [14], optical sensors [12,15] and mechanical arms [16,17]. Spatial calibration is required to accurately determine the relationship between the spatial sensor and the B-scan image plane. The position and orientation of the sensor at any point in space is calculated and recorded during the freehand scanning. The location of each B-scan image plane can be inferred using the spatial readings of the sensor. With accurate measurements of the spatial data for B-scan images recorded in a single examination, a 3D image formed by a regular voxel array can be reconstructed from B-scan pixels which are registered into the volume coordinate system. Due to its advantages of unlimited field of view and low cost, freehand scanning protocol has been proven to be the cheapest and the most flexible imaging tool in comparison with its competitors [2].

Using tracked freehand systems, some authors [18] performed data analysis without the need to create 3D volume data sets. In their work, the operations of extracting 3D contours were directly conducted using original B-scans, avoiding long computation time for volume reconstruction. However, the computer used in such a system would be equipped with a large amount of memory to store the original data and the analysis method would have to handle the very large amount of data, resulting in longer processing time in comparison with that based on a 3D volume data set with relatively lower resolution. In addition, the users may not be able to view the entire picture of the scanned body parts by inspecting all of the scattered B-scan images. To view internal part of the data, a reslicing procedure should be required, leading to much time for mapping pixels from the B-scans onto the slice plane. In comparison, reslicing of voxel arrays is straightforward and fast [18]. Therefore, as stated by Rohling et al. [19], volume reconstruction (interpolation of voxels) is normally a key procedure for most applications, and the interpolation errors and artifacts should be avoided and the important diagnostic information should be preserved well during the reconstruction.

In the past years, a number of interpolation algorithms for this problem have been reported. According to a previous survey [19], these interpolation methods for freehand 3D ultrasound could be grouped into three categories: voxel nearest neighbor (VNN), pixel nearest neighbor (PNN) and distance weighted (DW) interpolation. VNN method was easy to understand: each voxel value was assigned as the nearest pixel intensity. Although this method was easy to realize and offered the most original texture patterns from B-scan images, large reconstruction errors were usually generated within the gaps between B-scan image planes. PNN method assigned the intensity of each pixel to its nearest voxel grid point and averaged multiple contributions to a single voxel. This method however causes great blurring as well as relatively large reconstruction error. In comparison, DW method was able to further reduce reconstruction error, suppress speckle noises and preserve image details. For each voxel, the neighboring pixels in a predefined fixed spherical region were weighed with respect to their inverse distances to the voxel centre and then averaged. Because of the averaging operation, the DW method has been traditionally considered being good at reduce speckles [20]. This method could provide improved image quality and reduced reconstruction errors in comparison with VNN and PNN methods [19, 21]. Based on the concept of DW, several interpolation algorithms were reported to reduce the reconstruction error and improve the 3D image quality in recent years [21-23]. In particular, a weighted ellipsoid Gaussian convolution kernel using similar computation principle to conventional DW method was applied to the neighboring pixels of each voxel in volume reconstruction, and obtained 3D images with more texture patterns and small resolvable objects [21,23].

However, no attention from aforementioned studies was paid to developing an interpolation scheme which can both suppress speckle noises and preserve important anatomical features. As is well-known, speckle is an undesirable property of B-mode ultrasound imaging because it may mask small but diagnostically significant features. Lots of efforts have been made to reduce speckles and preserve important edge details in conventional medical ultrasound images [24-28]. In some of these studies, the ratio of variance to mean in a local region has been thought of as a metrics to determine whether or not the region can be classified as a homogenous speckle region. Despite the unclear theoretical validity of this method, some previous authors have experimentally demonstrated its usefulness in differentiating the significant edges from homogeneous speckle regions [24-26]. Using the ratio, adaptive distance-weighted (ASDW) interpolation methods have been proposed to reduce speckle noises and preserve tissue edges in reconstruction of freehand 3D ultrasound images [29, 30]. Although improved 3D images could be obtained, the interpolation of voxels required an extremely large amount of storage capacities and hence resulted in a less efficient computation and even an infeasibility of reconstruction for the PCs without enough RAM memory. To the best of our knowledge, little attention has been paid to the reduction of the computer memory occupied for the volume reconstruction in freehand 3D ultrasound imaging.

In this study, we proposed a new adaptive algorithm called adaptive Gaussian distance weighted (AGDW) interpolation for reconstructing 3D freehand ultrasound images with reduced speckle noise and well preserved diagnostic features. In order to reconstruct a large voxel array in a PC, a novel method was also proposed to perform the reconstruction slice by slice with an economical usage of memory, being more practical than previously proposed algorithms for the PC-based applications. The local statistics (mean and variance) were measured and the ratio of variance/mean was calculated in 3D speckle regions. The relationship between the homogeneity of speckle region and region size was investigated. We employed the same registration procedure for B-scan pixels and a spherical neighbouring region for each voxel grid point as used by conventional DW method. If a voxel's neighbouring region with default size was inhomogeneous, a Gaussian convolution kernel with an adaptive parameter in relation to the ratio of local variance/mean was applied. Otherwise, the size of the neighbourhood for the voxel was contracted and whether it was lying within a homogenous region or near edges would be re-judged. Once its neighbouring region was eventually considered being homogeneous, a trimmed mean filter was performed to reduce speckles. The next section describes the reconstruction algorithm and experimental methods in detail. Consequently, the preliminary results obtained from an ultrasound resolution phantom and real human tissues are presented. The discussion and conclusion for the proposed method are finally given in this paper.

2. Methods

2.1. System description

In this study, a previously developed freehand 3D system [22] was used for data acquisition and volume reconstruction. The system was comprised of an electromagnetic spatial sensing device (miniBird, Ascension Technology Corporation, Burlington, VT, USA), a portable ultrasound scanner (SonoSite 180PLUS, SonoSite, Inc., Bothell, WA, USA), and a personal computer (PC) with a 3.0 GHz Pentium IV processor and 1 GB of RAM. A custom-designed software system programmed in VC++ was designed for data collection, volume reconstruction, visualization and data analysis. The receiver of the spatial sensing device was attached to the 7.5 MHz linear array probe of the ultrasound scanner. The video stream of the ultrasound scanner was digitized by a video capture card (NI-IMAQ PCI/PXI-1411, National Instruments Corporation, Austin, TX, USA) installed in the PC. The position and orientation of the spatial receiver could be simultaneously recorded through RS232 serial port. After a temporal calibration procedure [22], the B-scans with a pixel resolution of 0.08 mm were matched to the spatial data points at 20 Hz.

Spatial calibration using a cross-wire phantom [13, 31] was performed to determine the spatial relationship between the receiver and the ultrasound probe.

2.2. Measurements of speckle statistics

The statistics of speckle in ultrasound images has been discussed by many authors in past decades [24-26]. A signal-dependent noise model for speckle specification is widely used to identify speckle regions in ultrasound images [24]. This model indicates that the variance is proportional to the mean in a homogenous speckle region. Thus, the ratio of variance/mean can be used as a criterion to determine whether a local region is homogenous or not.

Traditional techniques for speckle reduction required a pre-specified, image-dependent constant homogeneity as a threshold value. However, the homogeneity of speckle region actually varied with the size of the region measured according to a previous study [25]. In this study, we recorded several sequences of parallel B-scans with different spacings in a regular manner and measured local speckle statistics in 3D spherical regions with different radiuses, as demonstrated in Fig. 2. A 3D translating device (Parker Hannifin Corporation, Irvine, CA, USA) was employed to conduct the linear scanning on an ultrasound resolution phantom (Model 44, CIRS Inc, USA) and part of a healthy male subject’s forearm. Fig. 3 illustrates two typical 2D ultrasound images captured from the phantom and the subject. Five different spacings of the B-scan sequences were chosen to be 0.04 mm, 0.08 mm, 0.16 mm, 0.32 mm, and 0.64 mm, respectively. Within each set of B-scans, the local statistics of 10 spherical regions at different locations containing only speckles were measured. The averaged ratios of variance/mean under different region sizes and spacing conditions are summarized in Table 1 and Table 2 for the resolution phantom and real tissues, respectively. Whether the size of speckle region and the spacings of B-scan had significant effects on the measures of local variance/mean was evaluated using Two-way ANOVA (MiniTab, MiniTab Inc., PA, USA). Both of the two P-values that we obtained are 0.0 (<0.01), indicating that both of the radius of spherical region and the spacings of B-scan sequence resulted in significant difference for speckle measurements of the resolution phantom and real human tissues. Fig. 4 demonstrates the measured results of local speckle statistics. Because the numerical difference caused by the B-scan spacings was very small, we studied only the resulting effect of the radius of spherical region. For the phantom and musculoskeletal tissues of the subject, the effect of the size of speckle region could be delineated by two logarithmic trendlines with small approximation errors (R^2>0.97). Thus, the two trendlines shown in Fig. 4 were used as dynamic threshold values to detect homogenous regions in this study.

2.3. Interpolation algorithm

In each experiment, a region of interest was scanned in a single sweep with a slow and steady motion using the freehand system. Fig. 1 illustrates the outline of a sequence of B-scans in a typical sweep. A regular voxel array was defined with respect to the distribution of B-scan pixels in 3D space. Being similar to conventional DW interpolation, our algorithm proceeded voxel by voxel. A default spherical neighbourhood with a radius of R_{max}, centred about each voxel was predefined. The intensities of B-scan pixels transformed into this neighbourhood and their distances to the voxel centre were stored in a dynamic array in association with the current voxel.

For reconstruction of voxels, the following interpolation algorithm including two main steps was proposed in this paper. The first step was to determine whether or not a voxel was locating in a homogenous region. With the default size of neighborhood (R=R_{max}) for each voxel, the local statistics including the variance and mean was calculated. If the local ratio of variance/mean was below the threshold value in association with the size of speckle region, the current voxel was considered locating in a homogenous speckle region. Otherwise, a B-scan pixel's resolution, R_p, was subtracted from the radius (R) of its neighborhood, i.e. R=R-R_p. Within the shrunken neighborhood, the statistics of pixels was calculated again and the homogeneity threshold updated by the decreased radius was used to judge whether or not the contracted neighborhood was a speckle region not containing an object edge. This contraction of neighborhood radius did not stop until the ratio of local variance/mean was no larger than the updated homogeneity threshold, the remaining pixel number in the updated neighborhood was less than a pre-set threshold (P_t), or the neighborhood radius reached a pre-set minimum value (R_{min}). For the latter two cases, the neighborhood radius was expanded with an increase of R_p, i.e. R=R+R_p. In this study, P_t was set to 5 and R_{min} was set to the voxel width. This step is summarized in Fig. 5.

The second step was to compute voxel values with respect to the local statistics. Once a voxel was deemed as locating in a homogeneous background, a trimmed mean filter was applied to compute the voxel value. For a voxel locating at (i, j, k) in the voxel array, the calculation of its value was expressed by

$$V(i,j,k)=\frac{1}{N_t}\sum_{P_l\in T}P_l\ ,$$

$$T=\{P_l \mid l\in S\cap|P_l-\mu_S|<\sigma_S\} \quad (1)$$

where P_l was the lth pixel intensity within the voxel neighborhood S, μ_S and σ_S were the mean and standard deviation of all pixels in S, respectively, T was the pixel set only containing pixels within one standard deviation of the mean, N_t was the number of pixels in T, and $V(i, j, k)$ was the output voxel value.

On the contrary, if the voxel was treated as locating at an inhomogeneous region, we employed a Gaussian convolution kernel related to the local ratio of variance/mean in its neighborhood. The output value of voxel (i, j, k) was computed as follows,

$$V(i,j,k)=\frac{\sum_{m=0}^{n}W_mP_m}{\sum_{m=0}^{n}W_m}\ ,\ W_m=e^{-\left(\frac{\sigma_S{}^2}{\mu_S}-H_c\right)\frac{d_m^2}{b}} \quad (2)$$

where P_m was the mth pixel value in the neighborhood of voxel (i, j, k), d_m was the distance between P_m and the voxel center, H_c was the radius-based homogeneity of the voxel neighborhood, W_m was the weight in association with P_m in this weighted mean filter, and b was a parameter empirically set by the operator. Because an adaptive Gaussian convolution kernel method was employed for interpolation of voxels in inhomogeneous regions, this proposed algorithm was named as adaptive Gaussian distance weighted (AGDW) interpolation in this paper.

2.4. Volume reconstruction with an economical memory usage

The proposed volume reconstruction method required that a dynamic pixel array storing neighboring pixel intensities should be associated with each voxel. However, if there were a large number of raw B-scans or the voxel size was set as small as the pixel size, the memory of the PC would be quickly overwhelmed and the failure of reconstruction would result. To make our reconstruction algorithm feasible for real practices, we proposed a novel procedure for volume reconstruction with economical memory usage.

The reconstruction was carried out slice by slice. In this study, the voxel array was considered as a set of 2-D slices along *z*-axis, i.e. the scanning direction as demonstrated in Fig. 1. As illustrated in Fig. 6, we defined a neighbouring cuboid which could merely contain the voxels on one slice and their neighbourhoods. In another word, the cuboid could be generated by expanding the voxel grids along six directions by the default neighbourhood radius used for volume reconstruction. For each slice, only B-scans intersecting its neighbouring cuboid were loaded into the memory allocated to the current slice. The pixels from these B-scans were transformed into the volume coordinate system and stored in the pixels arrays of all voxels on the slice. Once the slice was completely reconstructed, the memory allocated for storing these pixel arrays was released and the next slice would be reconstructed in the same way.

A critical problem was, however, how to determine which B-scans intersected the neighbouring cuboid for each slice. In this study, this problem was solved by the following procedure. Within the volume coordinate system where the direction of *z*-axis was set to be the same as the *z*-axis of the volume data set, we assumed that the range of the cuboid of a slice perpendicular to the *z*-axis was defined by (X_{min}, X_{max}), (Y_{min}, Y_{max}), and (Z_{min}, Z_{max}) along the three axes (x, y, z), as shown in Fig. 6. All B-scans in an examination were tested if they were intersecting the cuboid. The following rule was proposed to judge if a B-scan plane with four vertices intersected the cuboid.

IF *the z-values of all vertices of the B-scan* $< Z_{min}$ ***THEN*** *the B-scan did not intersect the cuboid;*

ELSE IF *the z-values of all vertices of the B-scan* $> Z_{max}$ ***THEN*** *the B-scan did not intersect the cuboid;*

ELSE IF *the x-values of all vertices of the B-scan* $< X_{min}$ ***THEN*** *the B-scan did not intersect the cuboid;*

ELSE IF *the x-values of all vertices of the B-scan* $> X_{max}$ ***THEN*** *the B-scan did not intersect the cuboid;*

ELSE IF *the y-values of all vertices of the B-scan* $< Y_{min}$ ***THEN*** *the B-scan did not intersect the cuboid;*

ELSE IF *the y-values of all vertices of the B-scan* $> Y_{max}$ ***THEN*** *the B-scan did not intersect the cuboid;*

ELSE IF *all vertices of the cuboid were locating at one side of the B-scan plane* ***THEN*** *the B-scan did not intersect the cuboid;*

ELSE *the B-scan did intersect the cuboid.*

Using this rule, only those B-scans intersecting the voxel neighborhoods were used to interpolate the current slice. This would result in relatively faster computation and reduced memory allocation.

2.5. Experimental methods

The ultrasound resolution phantom was scanned in this study. A set of 110 nearly parallel B-scans were captured in a single sweep. Each B-scan was cropped to 506×378 pixels. A voxel array with 131×113×110 voxels was reconstructed using conventional DW, VNN, Gaussian convolution kernel, and AGDW methods, respectively. For the DW, Gaussian and AGDW methods, a spherical region with a default radius of 0.4 mm was predefined for each voxel. The parameter b in the AGDW method was set to 0.5. The homogeneity threshold H_c for the resolution phantom was determined in relation to the radius as shown in Fig. 4(a). Totally, 4 voxel arrays using these methods were reconstructed in this phantom study.

Four representative slices were chosen from the same location in the voxel arrays reconstructed using the DW, VNN, Gaussian and AGDW (b=0.5) methods. To compare the performance in speckle suppression and edge preservation among the four different methods, the signal-noise-ratio (SNR) of the 3-D homogeneous regions and the local contrast of target regions (see Fig. 3 (a)) interpolated using these methods were studied. We selected 4 homogenous sub-volumes at the same location only containing speckles from the 4 voxel arrays, respectively. Their SNRs was computed for comparing the performances in reducing speckles among the four reconstruction methods. Larger SNR values indicated better performance in speckle reduction. In addition, local contrast measure [32] was also conducted to compare the performance of edge preservation using these different methods. For a voxel $V(i, j, k)$ at the coordinates (i, j, k) in a voxel array, the local contrast in its $2n$+1 neighbourhood can be expressed as:

$$C(i,j,k)=\frac{Max(I_s(i,j,k))-Min(I_s(i,j,k))}{Max(I_s(i,j,k))+Min(I_s(i,j,k))}, \tag{3}$$

where $I_s\,(i, j, k)$ denotes a group of voxel intensities at the location (i, j, k) and the voxel's neighbourhood. We used the averaged local contrast in a 3-D inhomogeneous region to represent the performance of contrast enhancement. The method is described by

$$C_A = \frac{\sum_{(i,j,k)\in S} C(i,j,k)}{N_v}, \qquad (4)$$

where S is a sub-volume cropped from a reconstructed volume, and N_v is the voxel number within the sub-volume. In this phantom study, another 4 sub-volumes with mainly including a typical dark target were selected at the same location from the 4 voxel arrays, as illustrated in Fig. 3(a). The averaged local contrast measures were applied to the selected sub-volumes at the same location. It is noted that sharper edges, more texture objects and details in raw B-scans would be preserved in a sub-volume with a larger C_A.

Besides the phantom study, an *in vivo* examination was performed on the healthy male subject's forearm. The subject gave his informed consent to the investigation which was approved by the Hong Kong Polytechnic University Human Subjects Ethics Committee. A dense set of 188 nearly parallel B-scans was captured and each B-scan was cropped to 408×305 pixels. The homogeneity threshold (H_c) for this *in vivo* experiment was determined with respect to the spherical neighbourhood radius, as measured in Fig. 4(b). An evaluation test previously introduced by Rohling et al. [19] was carried out in this *in vivo* study. The idea of the test was to evaluate the ability of a reconstruction technique in preserving true intensity values at the locations where a part of original data was removed. A good reconstruction method should be able to interpolate the removed grid points with values very close to the original data. A B-scan near the middle of the raw data set was selected for pixel removing. Different percentages of pixels were removed randomly from this selected B-scan. The remained data were used to reconstruct a voxel array with a voxel size equivalent to the pixel size. The average of the absolute differences between the interpolated grid points and the missing original pixel values was calculated for evaluating the reconstruction performance using the following equation:

$$V = \frac{1}{N}\sum_{i=1}^{N}\left|p_i - r_i\right| \tag{5}$$

where p_i is the removed original pixel intensity, r_i is the interpolated intensity at the location of p_i, and N is the number of removed pixels. A smaller V indicates a better performance of interpolation. Seven different data removing ratios were used in our tests, i.e. 25%, 50%, 75%, 100%, 300%, 500% and 700%. The tests with the data removing ratios of 25%, 50%, 75% and 100% were performed using the selected B-scan *n*. For the 300% test, the data from the B-scan n±1 and B-scan *n* were removed. The 500% and 700% tests further removed all data from the B-scan n±2 and n±3, respectively. In this evaluation method, the default radius of predefined neighbourhood for each voxel was 0.5 mm for the 25%, 50%, 75% and 100% tests, 0.8 mm for the 300% test, 1.1 mm for the 500% test, and 1.4 mm for the 700% test. The averaged interpolation error from 10 randomly selected B-scans was recorded to compare the performance of the proposed AGDW method (b=0.5) with that of the other three often used methods, i.e. the DW, VNN and Gaussian methods.

3. Results

Fig. 7 demonstrates a set of reconstructed slices of the ultrasound resolution phantom using the DW, VNN, Gaussian, and AGDW (b=0.5) methods, respectively. It can be observed that the proposed AGDW method reduced most of speckles in homogeneous regions and effectively preserved the edges of the round targets (Fig. 7(d)). In comparison, the DW method blurred the target edges (Fig. 7(b)) and the VNN seemed to overemphasize the original texture patterns of ultrasound images (Fig. 7(a)). The Gaussian method presented an improvement in edge preservation but retained most of speckle characteristics in the slice.

Table 3 presents the quantitative results for the SNR and the averaged local contrast measurements. The AGDW method offered similar SNR result to the DW method, indicating a good performance in suppressing speckles. As the DW method has proven to be good at speckle suppression, it offered the best SNR result. The Gaussian method preserved relatively more speckles in comparison with the DW and AGDW methods. It is obvious that the VNN method preserved most of the speckle patterns in homogeneous regions. For the averaged local contrast measure, the proposed AGDW method produced higher contrast than the DW and Gaussian method in the edge regions, indicating a good improvement in edge preservation. Although the VNN method produced the largest value of local contrast, it introduced most of noises and preserved most of speckles in the image, giving the lowest SNR value and hence showing the worst image quality.

The result for the data removing test is summarized in Fig. 8. The VNN method generated the largest interpolation error though it preserved the most texture patterns. Due to the greatest level of misalignments for relatively large gaps between B-scans, the VNN method generally had greater reconstruction error than the other conventional methods [19, 21, 31]. The DW method produced improved interpolation quality compared with the VNN. The proposed AGDW method (b=0.5) further reduced the interpolation error, illustrating a good interpolation performance. In comparison, the Gaussian method offered the best interpolation result, since it preserved many speckle patterns in homogenous regions but the AGDW over-smoothed these image contents.

Fig. 9 shows four typical slices reconstructed using the DW, VNN, Gaussian and AGDW (b=0.5) methods, respectively, at the 100% evaluation test. The AGDW presented the most contrast at edge regions and smoothed most of speckles in comparison with other conventional methods. Fig. 10 demonstrates a quantitative comparison between different methods by extracting the intensities along column 200. It can be observed that the DW and Gaussian methods smoothed many small resolvable objects as well as significant edges, while the AGDW method gave a better contrast for the edges and made the boundaries easy to be identified. In comparison with the VNN method, the AGDW method did much better in reducing speckles and other noises. Although the reconstruction results using the VNN method seemed to be able to preserve most of texture patterns as shown in Fig. 9 (a), the noises were at the same time retained and hence the tissue boundaries were difficult to be contoured.

Fig. 11 highlights a smaller region of the removed image plane using the four methods at the 500% data removing test. They were qualitatively compared in this figure. The image content of the VNN was actually copied from the nearest unremoved B-scan, thus the largest interpolation error was produced as shown in Fig. 8. The DW method over-smoothed almost all small details of original image, making significant edges difficult to be identified. In comparison with the DW method, the Gaussian method greatly improved the reconstruction quality and offered the lowest interpolation error as shown in Fig. 8. Although the proposed AGDW method produced relatively larger interpolation error than the Gaussian method, it preserved significant edges well and reduced nearly all of speckles. This result indicates that the AGDW performed well in preserving edges and reducing interpolation error when the B-scan spacing was large.

4. Discussion and conclusion

In this study, an adaptive volume reconstruction algorithm was proposed for freehand 3D ultrasound imaging. This algorithm was designed to reduce speckles and preserve edges using local statistics of speckle. The ratio of local variance/mean was used as a criterion for determining whether the neighborhood of a voxel was homogenous or not. A study was performed to obtain the effects of the neighborhood radius and the B-scan spacing on the speckle statistics in 3D. With respect to the findings for speckle properties, the neighborhood for each voxel could be classified as homogeneous or inhomogeneous region. The voxels locating in homogeneous regions were computed using a trimmed averaging method to greatly reduce speckle noises. The other voxels which were regarded locating in inhomogeneous regions were interpolated using an adaptive Gaussian convolution kernel applied to their neighborhoods. In this adaptive method, the local variance/mean was a factor to adjust the interpolation result. Larger ratio of variance/mean in a local region would result in a Gaussian convolution kernel with a smaller standard deviation, hence presenting a better capability of preserving edges and small resolvable objects. In addition, a novel procedure for reconstructing the voxel array slice by slice was proposed to reduce the memory usage in the PC. Although the total computation time using the proposed method was still longer than other conventional interpolation methods, the preliminary results have demonstrated that the reconstruction procedure could be used to compute a large voxel array in our system and the AGDW algorithm could effectively improve the quality of 3D ultrasound images with suppressed speckles and well preserved edges.

The measurements of local statistics demonstrated that the homogeneity of speckle regions in both the phantom and forearm images varied with the radius of the spherical region. A logarithmic approximation could be used to delineate the relationship between the local variance/mean and the region size, as shown in Fig. 4. With respect to the trend lines in Fig. 4, a threshold for differentiating speckle regions and inhomogeneous regions containing significant edges was obtained in the volume reconstruction. Generally, a voxel's neighbourhood was considered a homogeneous region if the ratio of variance/mean was below the threshold. Because the speckle statistics depend on the scanner specifications, the relationship between the homogeneity of speckle regions and the region size is varied for different ultrasound scanners. Also, the imaged materials can also affect the speckle statistics, and hence the homogeneity should be appropriately determined through enough tests. A follow-up study could be the adaptive selection of the threshold to optimize the reconstruction result.

It is well-known that tissue edges and other small anatomical points are important for clinical diagnosis. In particular, edge preservation is very important for segmentation of anatomical structures [9, 33-35], as the increased gradient at edge voxels can make an easier and more accurate tracing of tissue boundaries. Consequently, more accurate 3-D measurements, such as volume estimation [2, 18], can be realized for 3-D objects. Furthermore, the improvement of edge preservation would be useful for the registration of multiple sweeps [36-38], as tissue edges could be treated as anatomical landmarks and used for alignment of different sweeps. According to the preliminary results, the AGDW method presented well-preserved edges and more diagnostic features in inhomogeneous regions because the adaptation strategy using the local statistics and the contraction of voxel neighbourhood resulted in an effective enhancement of image gradient, hence an improved edge and feature preservation. The parameter b was actually a scale factor for adjusting the effect of the ratio of variance/mean on the interpolation. Theoretically, an extremely large value of b would lead to similar interpolation performance to a mean filter for inhomogeneous regions, since the standard deviation of the Gaussian convolution kernel would be large. Although the parameter b was empirically assigned as 0.5 in our *in vitro* and *in vivo* studies, it can be appropriately adjusted according to a variety of needs in real applications.

Because the local statistics of neighbouring pixels of each voxel must be measured prior to the interpolation of voxel values, the AGDW needed relatively longer computation time than the DW in our experiments. With further progress in computer technology, the time for volume reconstruction using the AGDW method could be anticipated to be significantly reduced in the near future. In addition, speckle statistics of imaged human tissues should be studied prior to real examinations, which would cause inconveniency for various clinical applications. Thus, one of our future tasks will be the investigation of the speckle statistics for different human tissues for providing a table which will be used for selecting appropriate homogeneity threshold for a specific examination. Moreover, the effect of the parameter b on different human tissues will be further quantitatively studied for optimizing the reconstruction results in real examinations.

In conclusion, we have presented an adaptive volume reconstruction technique based on local statistics for freehand 3D ultrasound imaging in this paper. This algorithm using an arithmetic mean filter and an adaptive Gaussian convolution method was proposed to interpolate a voxel array with suppressed speckle noises and preserved edges and other anatomical features. According to its improved interpolation performance in comparison with conventional methods, this new method is expected to be a useful 3D imaging technique for both research and clinical practices.

Acknowledgements

This work was supported by the Hong Kong Research Grant Council (PolyU 5332/07E), Shenzhen University Research/Development Fund (No.200843) and National Natural Science Foundation of China (No.60772147).

References

[1] Fenster A, Downey DB, Cardinal HN. Three-dimensional ultrasound imaging. Phys Med Biol 2001; 46: R67-99.

[2] Gee AH, Prager RW, Treece GM, Berman L. Engineering a freehand 3D ultrasound system. Pattern Recogn Lett 2003; 24: 757-77.

[3] Nelson TR, Pretorius DH. Three-dimensional ultrasound imaging. Ultrasound Med Biol 1998; 24: 1243-70.

[4] Smith SW, Pavy HG, von Ramm OT. High-speed ultrasound volumetric imaging system. 1. Transducer design and beam steering. IEEE Trans Ultra Ferr Freq Cont 1991; 38 (2): 100-8.

[5] Greenleaf JF. Three-dimensional imaging in ultrasound. J Med Syst 1982; 6(6): 579-89.

[6] Ledley RS, Golab TJ, Buas M, Arminski L. True 3-D stereo ultrasonography to make ultrasound more easily understood. In: Proc. 12th Annual Int. Conf. of the IEEE Engineering in Medicine and Biology Society, Philadelphia, PA 12: 211-212, 1990.

[7] Ledley RS. Three-dimensional imaging system. US Patent no.4747411 1988.

[8] McCann HA, Chandrasekaran K, Hoffman EA, Sinak LJ, Kinter TM and Greenleaf JF. A method for three-dimensional ultrasonic imaging of the heart *in vivo*. Dynamic Cardiovasc Imaging 1987; 1: 97-109.

[9] Richard WD, Grimmell CK, Bedigian K, Frank KJ. A method for three-dimensional prostate imaging using transrectal ultrasound. Comput Med Imag Grap 1993; 17 (2): 73-9.

[10] Djoa KK, De Jong N, Van Egmond FC, Kasprzak JD, Vletter WB, Lancée CT, Van Der Steen AFW, Bom N, Roelandt JRTC. A fast rotating scanning unit for real-time three-dimensional echo data acquisition. Ultrasound Med Biol 2000; 26 (5): 863-9.

[11] Nguyen-Dinh A, Mauchamp P, Felix N, Dufait R, Auclair P, Flesch A. Integrated mechanism based multiplane/3D ultrasonic imaging probes. In: Ultrasonics Symposium, 2001 IEEE; 2: 1147-50.

[12] Trobaugh JW, Trobaugh DJ, Richard WD. Three-Dimensional Imaging with Stereotactic Ultrasonography. Comput Med Imag Grap 1994; 19 (5): 315-23.

[13] Detmer PR, Bashein G, Hodges T, Beach KW, Filer EP, Burns DH, Strandness DE. 3D ultrasonic image feature localization based on magnetic scanhead tracking: in-vitro calibration and validation. Ultrasound Med Biol 1994; 20(9): 923-36.

[14] King DL, King DL, Shao MYC. 3-Dimensional spatial registration and interactive display of position and orientation of real-time ultrasound images. J Ultras Med 1990; 9(9): 525-32.

[15] Treece GM, Gee AH, Prager RW, Cash CJC, Berman L. High-definition freehand 3-D ultrasound. Ultrasound Med Biol 2003; 29 (4): 529-46.

[16] Geiser EA, Christie LG, Conetta DA, Conti CR, Gossman GS. A mechanical arm for spatial registration of two-dimensional echocardiographic sections. Catheter and Cardio Diag 1982; 8(1): 89-101.

[17] Baba K, Satoh K, Sakamoto S, Okai T, Ishii S. Development of an ultrasonic system for three-dimensional reconstruction of the fetus. J Perinet Med 1989; 17 (1): 19-24.

[18] Prager PW, Gee A, Berman L. Stradx: real-time acquisition and visualization of freehand three-dimensional ultrasound. Med Image Anal 1999; 3: 129-40.

[19] Rohling RN, Gee AH, Berman L. A comparison of freehand three-dimensional ultrasound reconstruction techniques. Med Image Anal 1999; 3: 339-59.

[20] Barry CD, Allot CP, John NW, Mellor PM, Arundel PA, Thomson DS, Waterton JC. Three-dimensional freehand ultrasound: Image reconstruction and volume analysis. Ultrasound Med Biol 1997; 23: 1209-24.

[21] San José-Estépar R, Martín-Fernándes M, Caballero-Martínes PP, Alberola-Lopes C, Ruiz-Alzola J. A theoretical framework to three-dimensional ultrasound reconstruction from irregularly sampled data. Ultrasound Med Biol 2003; 29: 255-69.

[22] Huang QH, Zheng YP, Lu MH, Chi ZR. Development of a portable 3D ultrasound imaging system for musculoskeletal tissues. Ultrasonics 2005; 43: 153-63.

[23] Meairs S, Beyer J, Hennerici M. Reconstruction and visualization of irregularly sampled three- and four-dimensional ultrasound data for cerebrovascular applications. Ultrasound Med Biol 2000; 26: 263-72.

[24] Huang QH, Zheng YP. An adaptive squared-distance-weighted interpolation for volume reconstruction in 3D freehand ultrasound. Ultrasonics, 2006; 44: E73-7.

[25] Loupas T, McDicken W, Allan P. An adaptive weighted median filter for speckle suppression in medical ultrasonic images. IEEE Trans Circuits Syst 1989; 36: 129-35.

[26] Chen Y, Yin RM, Flynn P, Broschat S. Aggressive region growing for speckle reduction in ultrasound images. Pattern Recogn Lett 2003; 24: 677-691.

[27] Karaman M, Kutay MA, Bozdagi G. An adaptive speckle suppression filter for medical ultrasonic imaging. IEEE Trans Med Imag 1995; 14: 283-92.

[28] Abd-Elmoniem Z, Youssef AM, Kadah YM. Real-time speckle reduction and coherence enhancement in ultrasound imaging via nonlinear anisotropic diffusion. IEEE Trans Biomed Eng 2002; 49: 997–1014.

[29] Tsantis S, Dimitropoulos N, Ioannidou M, Cavouras D, Nikiforidis G. Inter-scale wavelet analysis for speckle reduction in thyroid ultrasound images. Comput Med Imag Grap 2007; 31: 117-27.

[30] Huang QH, Lu MH, Zheng YP, Chi ZR. Speckle suppression and contrast enhancement in reconstruction of freehand 3-D ultrasound images using an adaptive distance-weighted method. Applied Acoustics. In press.

[31] Huang QH, Zheng YP. Volume reconstruction of freehand three-dimensional ultrasound using median filters. Ultrasonics 2008; 48 (3): 182-92.

[32] Sun QL, Hossack JA, Tang JS, Acton ST. Speckle reducing anisotropic diffusion for 3D ultrasound images. Comput Med Imag Grap 2004; 28: 461-70.

[33] Noble JA, Boukerroui D. Ultrsound image segmentation: A survey. IEEE Trans Med Imag 2006; 25: 987-1010.

[34] Zhang WY, Rohling RN, Pai DK. Surface extraction with a three-dimensional freehand ultrasound system. Ultrasound Med Biol 2004; 30: 1461-73.

[35] Treece GM, Prager RW, Gee AH, Berman L. Fast surface and volume estimation from non-parallel cross-sections, for freehand 3-D ultrasound. Med Image Anal 1999; 3: 141-73.

[36] Gee AH, Treece GM, Prager RW, Cash CJC, Berman L. Rapid registration for wide field of view freehand three-dimensional ultrasound. IEEE Trans Med Imag 2003; 22: 1344-57.

[37] Huang QH, Zheng YP. A new scanning approach for limb extremities using a water bag in freehand 3-D ultrasound. Ultrasound Med Biol 2005; 31: 575-83.

[38] Rohling RN, AH Gee, Berman L. Automatic registration of 3-D ultrasound images. Ultrasound Med Biol 1998; 24: 841-54.

FIGURE CAPTIONS

Fig. 1. A typical single sweep of freehand B-scans in volume coordinate system.

Fig. 2. Measurements of speckle statistics in several spherical regions with different radiuses. These spherical regions were locating within several sets of parallel B-scans with different spacings.

Fig. 3. Two typical ultrasound images collected from the ultrasound resolution phantom (a) and human musculoskeletal tissues (b). A target region in (a) and several speckle regions in (a) and (b) are indicated by circles.

Fig. 4. Relationship between the local ratio of variance/mean and the radius of 3D spherical homogeneous region. (a) Measurements on the phantom B-scans, and (b) measurements on the human forearm B-scans.

Fig. 5. Flow chart for detecting the 3D homogeneous neighbourhood of a voxel grid. Once the homogeneity (A or B) was determined, the calculation of its value was performed using the pixels within the updated neighbourhood.

Fig. 6. Reconstruction of a slice perpendicular to the z-axis in volume coordinate system. A neighbouring cuboid was defined. The B-scans intersecting this cuboid were loaded to interpolate the voxel values on the slice.

Fig. 7. Four slices reconstructed using the DW, VNN, Gaussian and AGDW (b=0.5) methods for the ultrasound resolution phantom: (a) the VNN, (b) DW, (c) Gaussian, and (d) AGDW (b=0.5) methods.

Fig. 8. The comparison of the interpolation errors among the results of DW, VNN, Gaussian and AGDW (b=0.5) methods in the evaluation test for interpolating missing data.

Fig. 9. Four slices reconstructed for the subject's forearm at the 100% test using the: (a) the VNN, (b) DW, (c) Gaussian, and (d) ADW (b=0.5) methods, with lines indicating the column 200 in the image.

Fig. 10. The comparisons of intensities along column 200 of the four slices for the subject's forearm: (a) the ADW (b=0.5) and VNN, (b) the ADW (b=0.5) and DW, (c) the ADW (b=0.5) and Gaussian.

Fig. 11. Four slices reconstructed using the (a) VNN, (b) DW, (c) Gaussian, and (d) AGDW (b=0.5) methods for the subject's forearm at the 300% test.

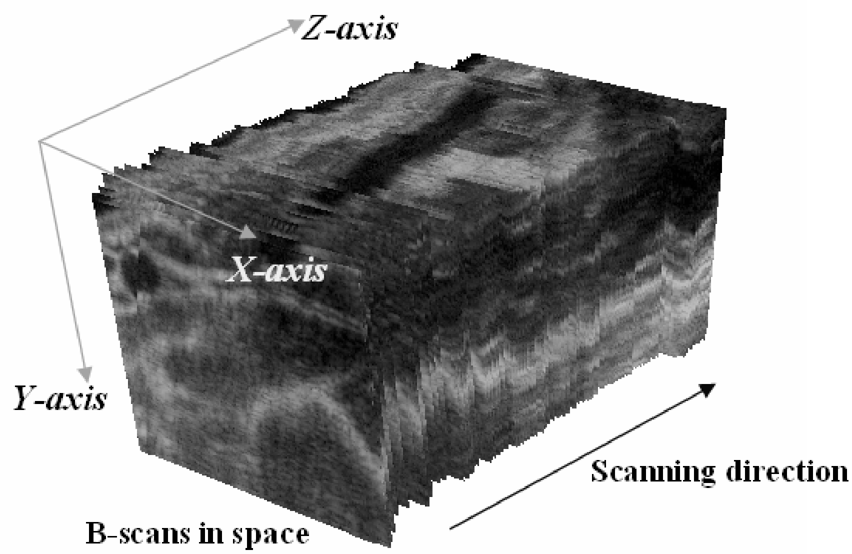

Fig. 1.

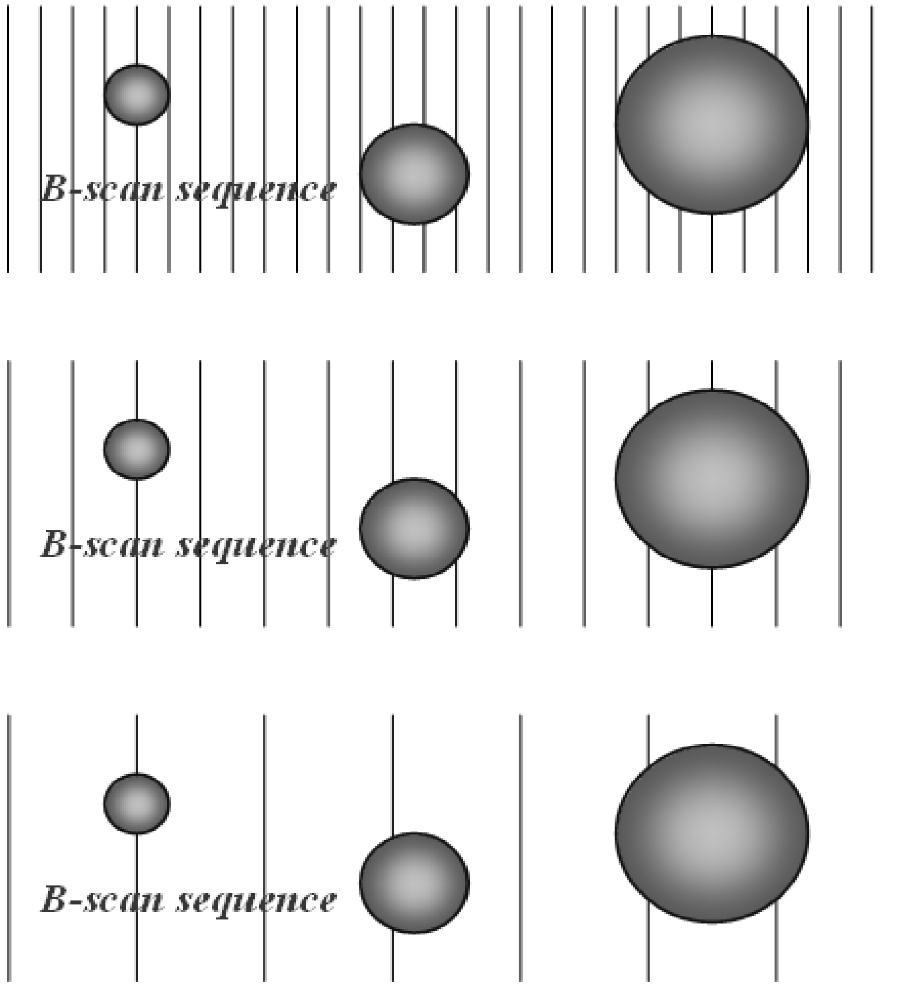
B-scan sequence
B-scan sequence
B-scan sequence

Fig. 2.

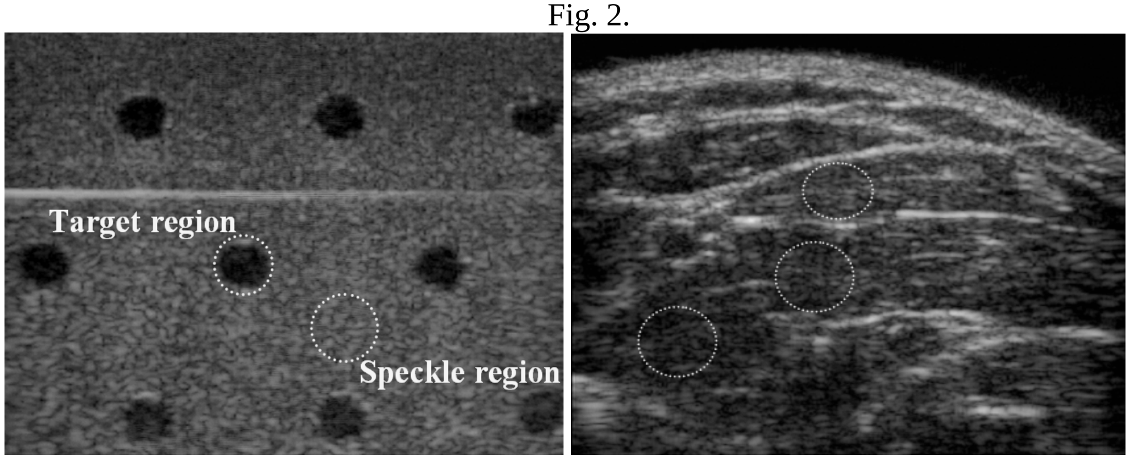
Target region
Speckle region

(a) (b)

Fig. 3.

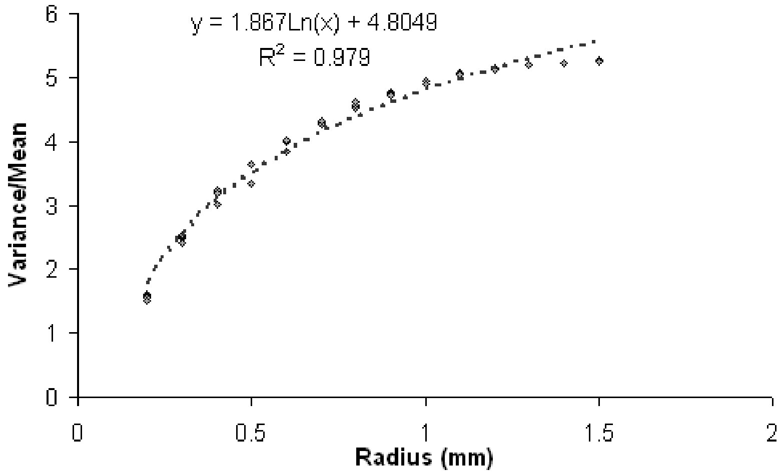
y = 1.867Ln(x) + 4.8049
R² = 0.979
Variance/Mean
Radius (mm)
0
1
2
3
4
5
6
0.5
1.5

(a)

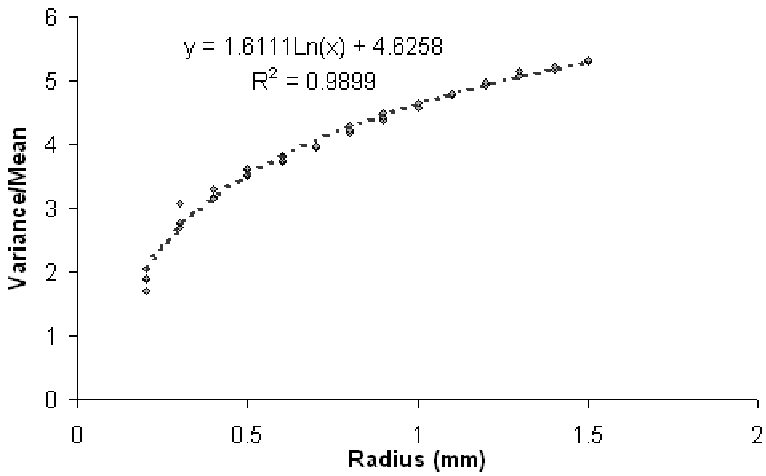
y = 1.6111Ln(x) + 4.6258
R² = 0.9899
Variance/Mean
Radius (mm)
0
1
2
3
4
5
6
0.5
1.5

(b)

Fig. 4.

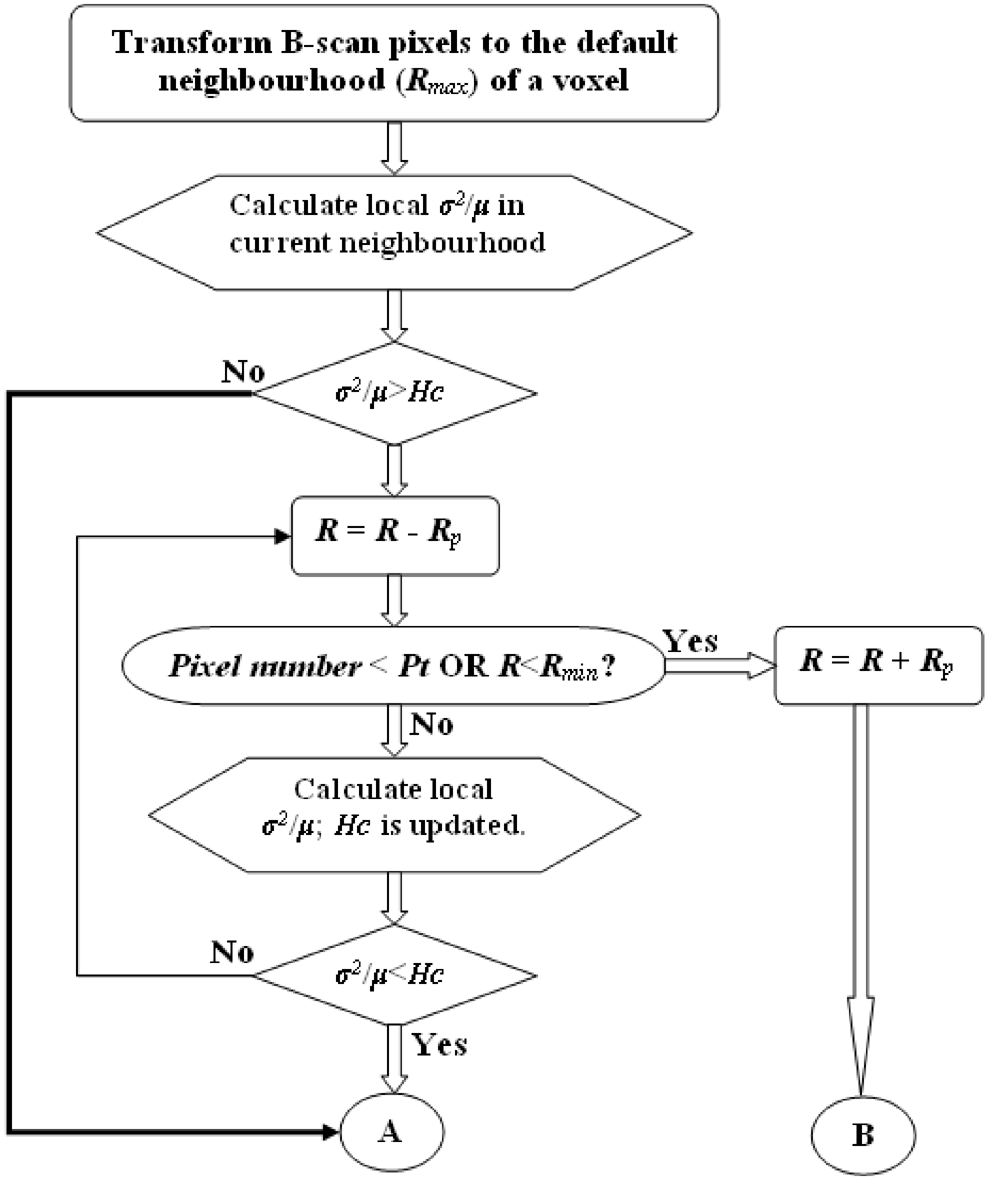

A: The voxel is considered locating in a homogeneous region.

B: The voxel is considered locating in an inhomogeneous region.

Fig. 5.

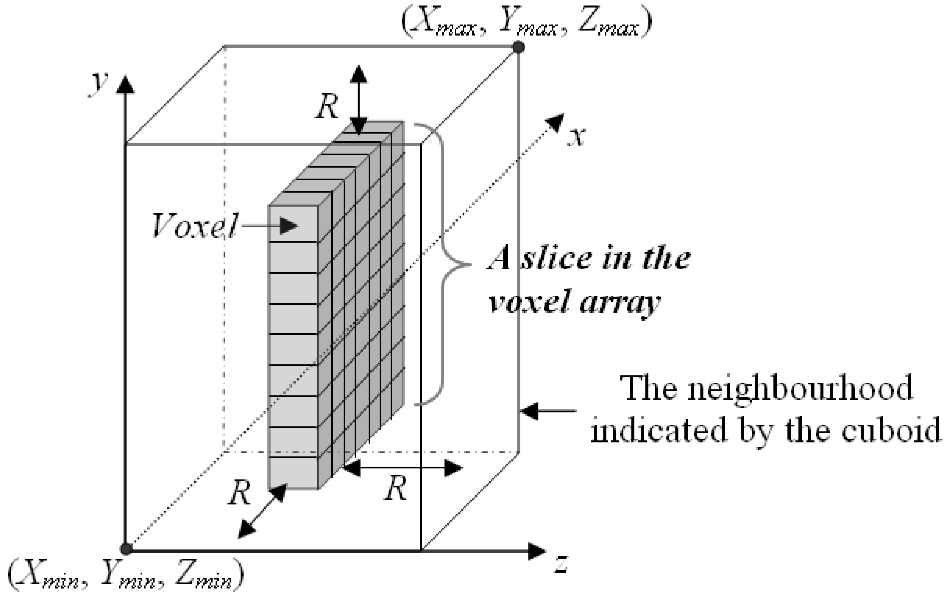

Fig. 6.

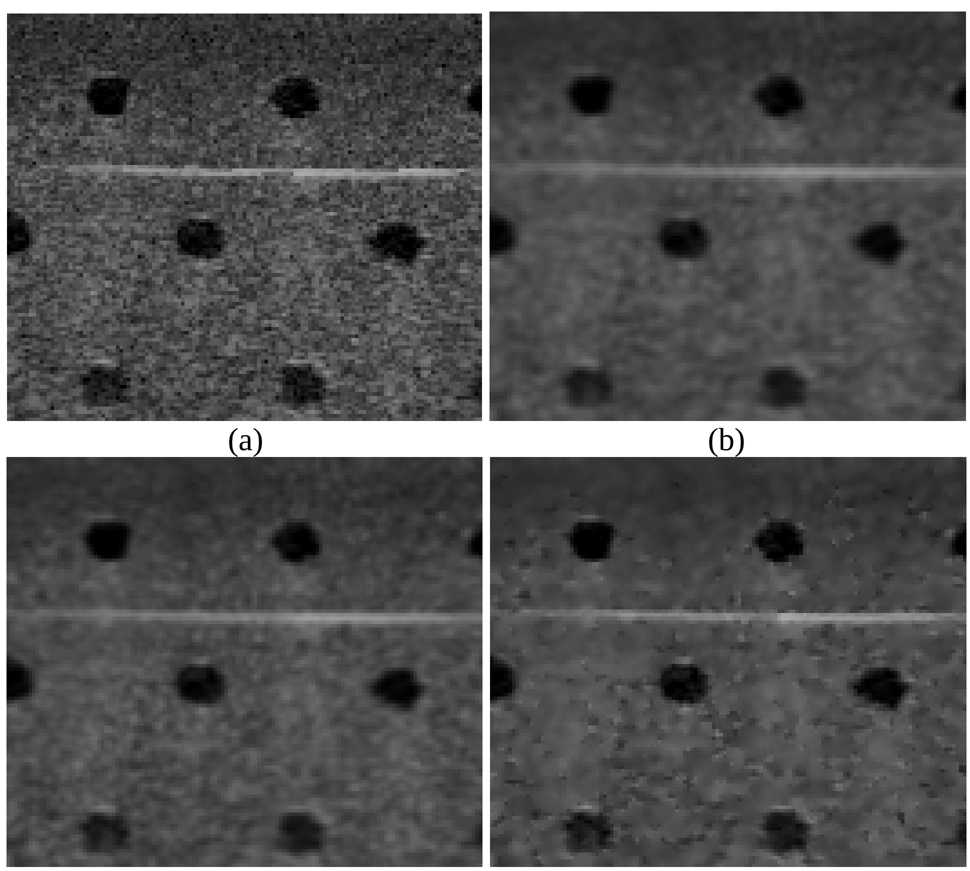

(a) (b)

(c) (d)

Fig. 7.

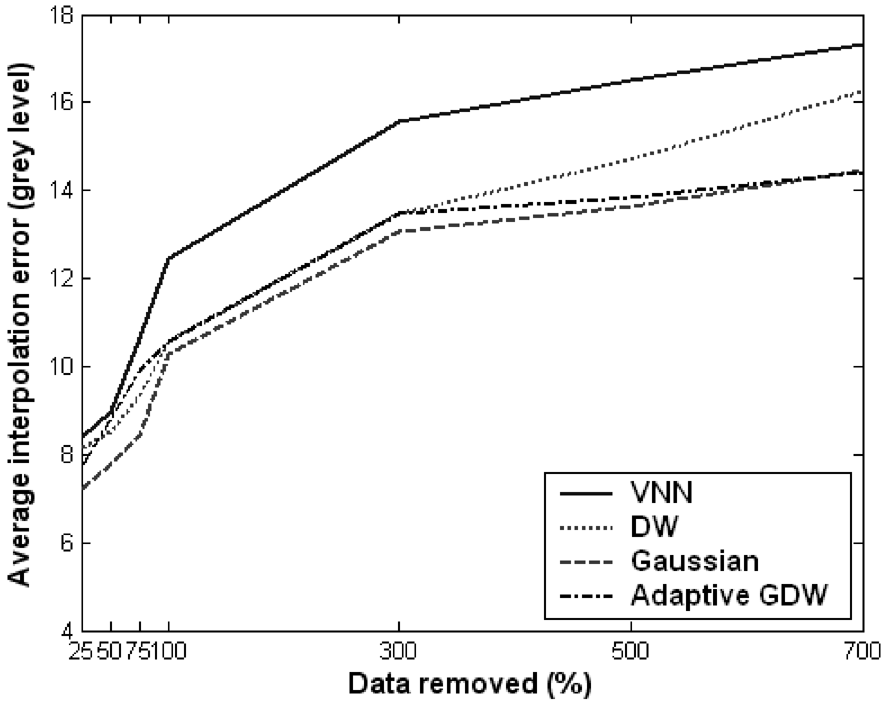

Fig. 8.

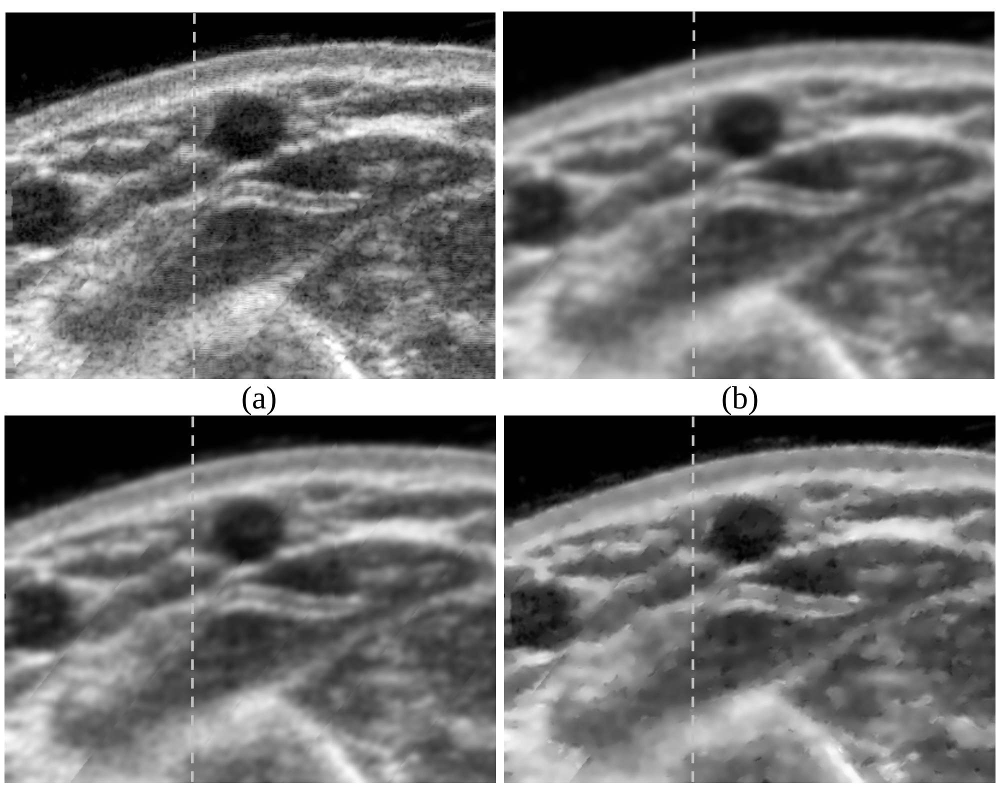

(a) (b)

(c) (d)

Fig. 9.

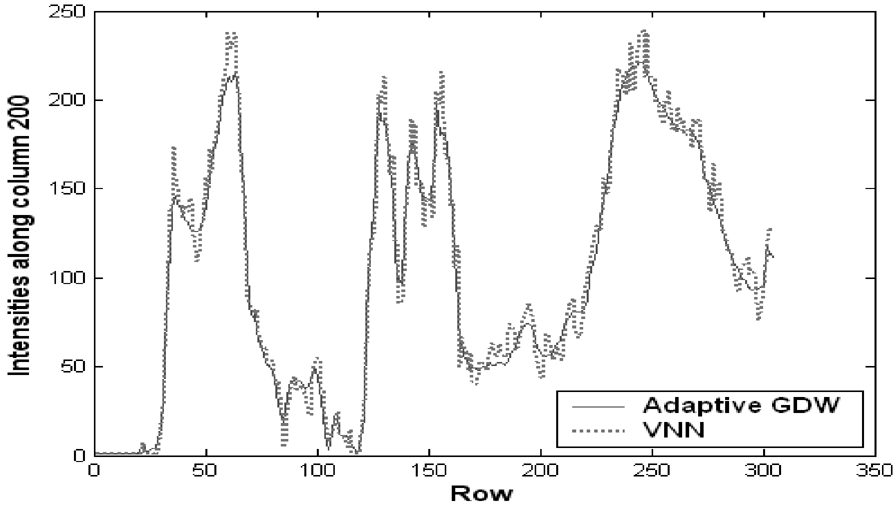
Intensities along column 200
Row
0
50
100
150
200
250
300
350
Adaptive GDW
VNN

(a)

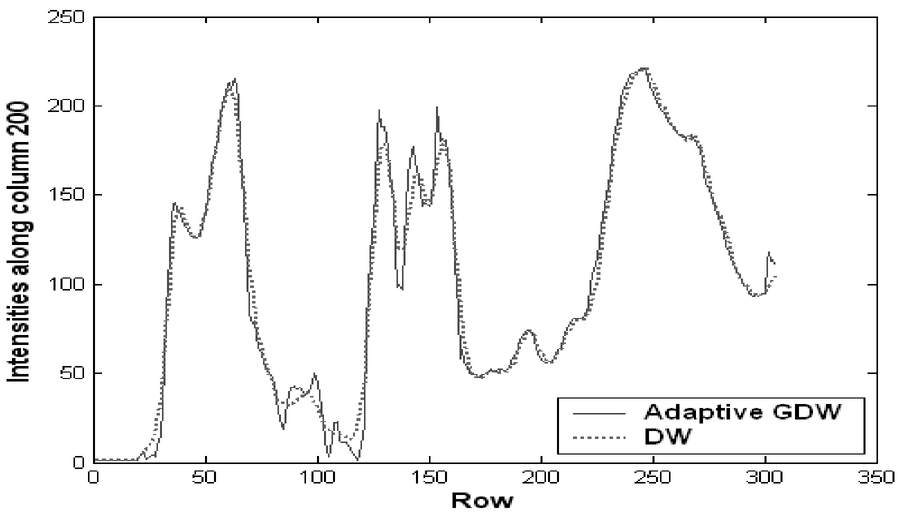
Intensities along column 200
Row
0
50
100
150
200
250
300
350
Adaptive GDW
DW

(b)

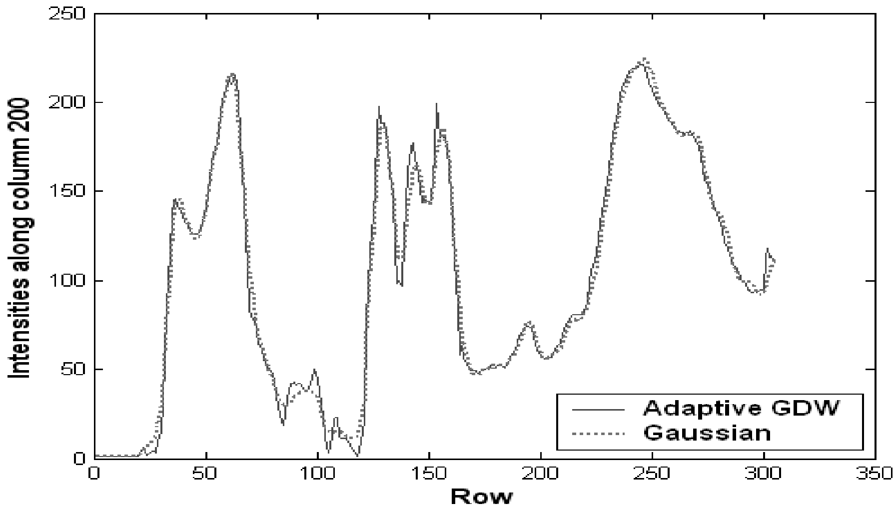

(c)

Fig. 10.

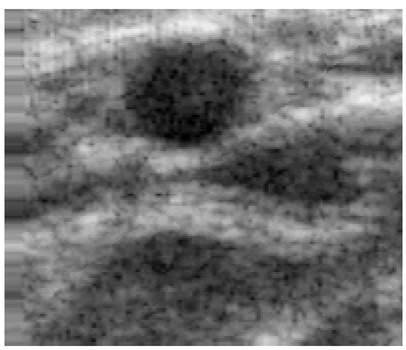

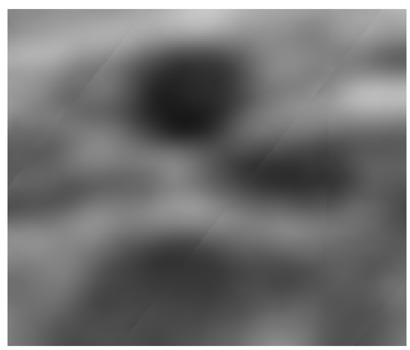

(a) (b)

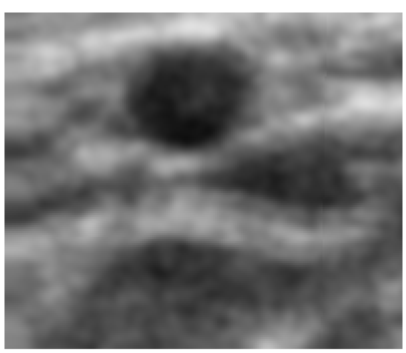

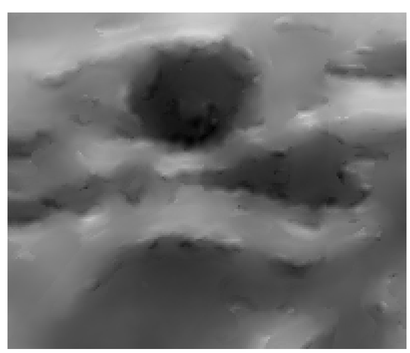

(c) (d)

Fig. 11.

TABLES

Table 1. Averaged local variance/mean in 3D homogeneous speckle regions with different radiuses (r) and spacings (s) for the resolution phantom.

r (mm)	Variance/Mean				
	s = 0.04 mm	s = 0.08 mm	s = 0.16 mm	s = 0.32 mm	s = 0.64mm
0.02	1.611	1.574	1.556	1.512	1.512
0.03	2.492	2.517	2.535	2.419	2.419
0.04	3.19	3.218	3.228	3.196	3.017
0.05	3.637	3.63	3.634	3.635	3.343
0.06	3.999	4.012	4.011	4.006	3.831
0.07	4.288	4.292	4.298	4.28	4.31
0.08	4.538	4.533	4.527	4.572	4.613
0.09	4.758	4.755	4.756	4.741	4.732
0.10	4.952	4.955	4.948	4.955	4.9
0.11	5.07	5.07	5.062	5.077	5.043
0.12	5.141	5.143	5.145	5.132	5.13
0.13	5.191	5.191	5.190	5.196	5.199
0.14	5.228	5.229	5.228	5.233	5.223
0.15	5.264	5.264	5.267	5.258	5.248

Table 2. Averaged local variance/mean in 3D homogeneous speckle regions with different radiuses (*r*) and spacings (*s*) for human musculoskeletal tissues.

r (mm)	Variance/Mean				
	s = 0.04 mm	*s* = 0.08 mm	*s* = 0.16 mm	*s* = 0.32 mm	*s* = 0.64mm
0.02	1.871	1.891	1.691	2.048	2.048
0.03	2.760	2.695	2.774	3.073	3.073
0.04	3.16	3.143	3.167	3.162	3.30
0.05	3.512	3.506	3.514	3.593	3.618
0.06	3.744	3.727	3.761	3.825	3.798
0.07	3.916	3.957	3.958	3.975	3.973
0.08	4.189	4.183	4.180	4.237	4.298
0.09	4.392	4.385	4.387	4.415	4.501
0.10	4.573	4.566	4.569	4.570	4.659
0.11	4.777	4.777	4.773	4.767	4.807
0.12	4.949	4.948	4.947	4.928	4.968
0.13	5.075	5.077	5.078	5.068	5.138
0.14	5.178	5.178	5.175	5.168	5.222
0.15	5.295	5.295	5.292	5.291	5.317

Table 3. Quantitative results of the phantom study for the measures of SNR in a homogeneous region and the averaged local contrast in a target region using different interpolation methods.

Metrics	DW	VNN	Gaussian	AGDW
SNR	9.273	5.612	8.861	9.266
Contrast	0.3554	0.6425	0.3951	0.4758